ACS APPLIED MATERIALS & INTERFACES

Research Article

www.acsami.org

High Proton Conductivity and Spectroscopic Investigations of Metal–Organic Framework Materials Impregnated by Strong Acids

Danil N. Dybtsev,[†,‡,§] Valentina G. Ponomareva,[‡,⊥] Sokhrab B. Aliev,[†] Alexei P. Chupakhin,[‡] Marsel R. Gallyamov,[†] Nikolay K. Moroz,[†] Boris A. Kolesov,[†] Konstantin A. Kovalenko,[†,‡] Elena S. Shutova,[⊥] and Vladimir P. Fedin*[,†,‡]

[†]Nikolaev Institute of Inorganic Chemistry, Siberian Branch of the Russian Academy of Sciences, 630090 Novosibirsk, Russian Federation

[‡]Department of Natural Sciences, Novosibirsk State University, 630090 Novosibirsk, Russian Federation

[§]Division of Advanced Materials Science, Pohang University of Science and Technology (POSTECH), Pohang 790-784, Republic of Korea

[⊥]Institute of Solid State Chemistry and Mechanochemistry, Siberian Branch of the Russian Academy of Sciences, 630128 Novosibirsk, Russian Federation

Supporting Information

ABSTRACT: Strong toluenesulfonic and triflic acids were incorporated into a MIL-101 chromium(III) terephthalate coordination framework, producing hybrid proton-conducting solid electrolytes. These acid@MIL hybrid materials possess stable crystalline structures that do not deteriorate during multiple measurements or prolonged heating. Particularly, the triflic-containing compound demonstrates the highest 0.08 S cm^{-1} proton conductivity at 15% relative humidity and a temperature of 60 °C, exceeding any of today's commercial materials for proton-exchange membranes. The structure of the proton-conducting media, as well as the long-range proton-transfer mechanics, was unveiled, in a certain respect, by Fourier transform infrared and ^{1}H NMR spectroscopy investigations. The acidic media presumably constitutes large separated droplets, coexisting in the MIL nanocages. One component of proton transfer appears to be related to the facile relay (Grotthuss) mechanism through extensive hydrogen-bonding interactions within such droplets. The second component occurs during continuous reorganization of the droplets, thus ensuring long-range proton transfer along the porous structure of the material.

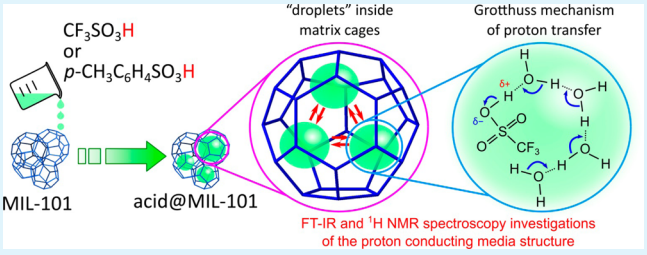

KEYWORDS: *metal–organic frameworks, proton conductivity, hybrid materials, spectroscopic investigations*

1. INTRODUCTION

The proton-exchange membrane (PEM) is an essential part of the fuel cell, allowing facile transport of H^+ ions from the anode to the cathode. The ion conductivity of the membranes limits the current generated by the fuel cell; therefore, materials with the highest possible proton conductivity are of great interest from both scientific and practical points of view.[1−13] The acid-doped poly(benzimidazole) membranes are the best materials operating at the moderate (100−200 °C) temperature range,[14,15] while perfluorianted Nafion and related organic polymers with strong acidic functions are today's state-of-the-art materials, demonstrating quite high proton conductivity at a low temperature range (up to 80 °C) and high humidity.[16,17] It is generally accepted that a prominent material for PEM should combine a high acid loading for efficient proton transfer, a cross-linking network for improved thermal and mechanical stability, and an enhanced surface area for effective electrical and chemical exchange with electrodes.[18] A novel approach to the design of highly conductive solid electrolytes based on porous coordination frameworks has been proposed[19] and developed.[20] Particularly, attempts at an acidity increase of the proton-conducting media by either direct framework functionalization[21−27] or inclusion of proton-conducting guest species into the pores[28−32] proved to be quite promising. In our most recent report,[33] we successfully impregnated mesopores of chromium(III) oxoterephthalate $[Cr_3O(H_2O)_3(bdc)_3]$ (MIL-101; bdc^{2-} = terephthalate, $C_8H_4O_4^{2-}$) by 2.7 M sulfuric and phosphoric acids without notable destruction of the coordination framework. The MIL-101 metal–organic structure possesses a highly open regular framework with large nanopores of ca. 30 and 38 Å diameter.[34] This work is a further development of such an approach reporting the incorporation of other strong acids, such as toluenesulfonic (p-$CH_3C_6H_4SO_3H$ or TsOH) and trifluoromethanesulfonic (CF_3SO_3H or TfOH) acid into MIL-101 at higher concentration in order to increase the number of mobile charge

Received: January 21, 2014
Accepted: March 17, 2014
Published: March 18, 2014

   dx.doi.org/10.1021/am500438a | ACS Appl. Mater. Interfaces 2014, 6, 5161−5167

carriers in the material. The obtained low-temperature proton conductivity of a solid TfOH-containing compound, 8×10^{-2} S cm^{-1}, at 60 °C and 3.5 mol % of water vapor [relative humidity (RH) ~ 15%] not only exceeds that of other known commercial PEM materials[16] but is less than an order of magnitude away from that of H_3PO_4, the compound with one of the highest intrinsic proton conductivities.[35,36] This work also put considerable effort into an investigation of the conductivity mechanism in the acid@MIL-101 hybrid materials by the Fourier transform infrared (FT-IR) and ^{1}H NMR spectroscopy. Our data provide important insight into understanding the role of the coordination nanospace in the structure of the aqueous medium and its influence on the proton conductivity pathways based on the extended hydrogen-bonding network.

2. EXPERIMENTAL SECTION

All chemicals and solvents were at least analytical grade and were used as purchased without additional purification.

2.1. Syntheses. *MIL-101.* A mixture of $Cr(NO_3)_3 \cdot 9H_2O$ (1.2 g, 3 mmol), terephthalic acid (H_2bdc; 500 mg, 3 mmol), 3 M HF (1 mL, 3 mmol), and water (15 mL) was added to a Teflon-lined steel autoclave, heated at a rate of 1 °C min^{-1} up to 220 °C, and kept at this temperature for 6 h. Then the mixture was slowly (less than 2 °C min^{-1}) cooled to room temperature. The crystalline precipitate, containing large colorless H_2bdc, and green microcrystals of MIL-101 were separated through a coarse glass filter, and then MIL-101 was filtered on a dense paper filter. The as-synthesized MIL-101 was purified by a double treatment in boiling ethanol (3 h per each treatment). Brunauer–Emmett–Teller (BET) surface area: 3200 m^2 g^{-1}.

TfOH@MIL-101 (1). MIL-101 (200 mg) was added to an aqueous solution (3.47 mL, 4,12 M) of trifluoromethanesulfonic acid (TfOH; Aldrich, 98%), and the suspension was stirred 30 min at room temperature. Then the solid product was filtered off using a glass filter and dried at room temperature for 24 h. Anal. Calcd for MIL-101·6.7TfOH·18H_2O ($C_{30.7}H_{60.7}Cr_3F_{20.1}O_{54.1}S_{6.7}$): C. 18.0; H. 3.0; S. 10.5. Found: C, 17.6; H, 2.7; S, 11.0. Inductively coupled plasma atomic emission spectroscopy (ICP-AES) data: the S/Cr ratio is 2.22.

TsOH@MIL-101 (2). MIL-101 (200 mg) was added to 3.6 mL of a 2.2 M aqueous solution of *p*-toluenesulfonic acid (TsOH·H_2O), and the suspension was stirred 30 min at room temperature. The solid product was filtered off, washed by 1 mL of water, and dried at 40 °C for 24 h. Anal. Calcd for MIL-101·1.1TsOH·2H_2O ($C_{31.7}H_{30.8}Cr_3O_{21.3}S_{1.1}$): C, 40.3; H, 3.1; S, 3.8. Found: C, 40.3; H, 3.3; S, 3.7. ICP-AES data: the S/Cr ratio is 0.37.

2.2. C, H, N, and S Analyses and ICP-AES Spectroscopy. Elemental analyses were obtained on a Eurovector 600 elemental analyzer. An ICP-AES spectrometer (iCAP 6000) was used to find the Cr/S ratio. Samples (20 mg) were dissolved in 10 mL of water with potassium hydroxide (150 mg) and hydrogen peroxide (0.5 mL, 30 wt % solution) and studied by ICP-AES afterward.

2.3. Thermogravimetric (TGA) and Thermocalorimetric Analyses. The thermal desorption study of guests was made on a simultaneous TG–DSC STA 449 F1 Jupiter apparatus with a Quadrupole MS 403C Aelous mass spectrometer (Netzsch GmbH, Germany) and Netzsch TG 209 F1.

2.4. BET Surface Area Measurements. The nitrogen sorption of MIL-101 was studied on a SORBTOMETER-M instrument. The samples were activated under a N_2 stream at 180 °C for 1 h.

2.5. Powder X-ray Diffraction (PXRD). PXRD data in a 2θ range of 2.5–30° were obtained on a Shimadzu XRD 7000S diffractometer (Cu Kα radiation, λ = 1.54178 Å).

2.6. FT-IR Spectra. FT-IR spectra of the samples in KBr pellet form were obtained on a Vertex 80 spectrometer. A liquid-helium Optistat cryostat from Oxford Instruments was used for recording the low-temperature spectra. The precision of the measured temperatures of the cold finger was 0.1 K. A stability of the temperature during measurement of better than 0.1 °C was provided by a temperature controller.

2.7. ^{1}H NMR Spectra. Measurements were carried out for sample **1** in the temperature range between 180 and 290 K at moderate magnetic field (0.55 T). The spectra were recorded in the form of the first derivative of the NMR absorption line by sweeping the frequency in the neighborhood of 23.5 MHz using a wide-line NMR spectrometer.

2.8. Conductivity Measurements. The compacted samples for conductivity measurements (pellets with 5.8 mm diameter and 1–2 mm thickness) were prepared by pressing the powders at 100 MPa. The alternating-current (ac) impedance measurements were carried out by a two-probe method using platinum-pressed electrodes with impedance meters (LCR-821 or Z-350M) in the frequency range above 1 Hz to 1 MHz. The measurements were carried out with a heating or cooling rate of 1–2 °C min^{-1} from ambient temperatures up to 115 °C in air at different humidity conditions: 0.6 and 3.5 ± 0.1 mol %. For sample **1**, the conductivity was also measured with constant 50% RH up to 60 °C. A water vapor partial pressure was controlled by air barbotage through a water saturator at definite temperature.

3. RESULTS AND DISCUSSION

The TfOH@MIL-101 (**1**) and TsOH@MIL-101 (**2**) proton-conducting hybrid compounds were prepared by soaking a MIL-101 crystalline powder in 4.12 M aqueous solutions of TfOH and 2.2 M toluenesulfonic acids, respectively. The PXRD patterns of **1** and **2** (Figure 1) coincide with the one of

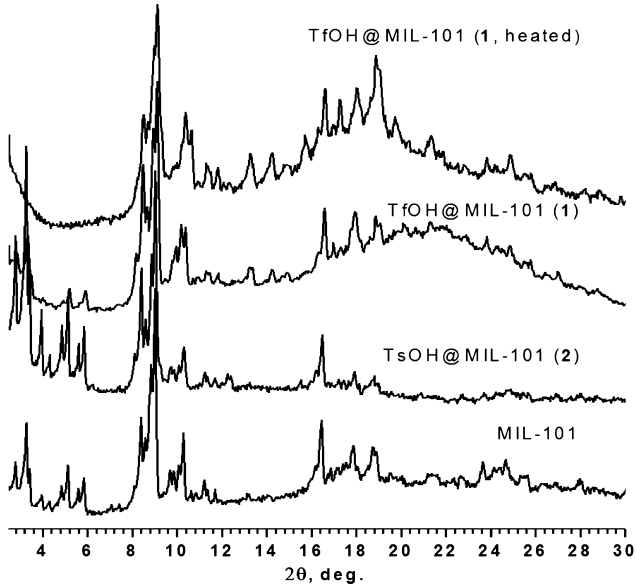

Figure 1. PXRD plots of (from bottom to top): MIL-101, as-synthesized TsOH@MIL-101 (**2**), as-synthesized TfOH@MIL-101 (**1**), and TfOH@MIL-101 (**1**), heated to 115 °C during the conductivity measurements. The spectral intensities are normalized by the strong reflection at $2\theta \approx 9°$.

starting MIL-101, proving the stability of the coordination host framework. A noticeable very broad maximum of the background of **1** could be attributed to the high amount of quasi-liquid (glassy) component in the MIL-101 pores. Elemental analysis and TGA further confirm the formation of hybrid host–guest materials with reasonable chemical composition. According to the data, the S/Cr ratio in **1** is 2.22, which is consistent with 6.7TfOH molecules per MIL-101 formula unit $[Cr_3O(bdc)_3(H_2O)_3]^+$ or 76TfOH molecules per MIL nanocage. TGA data for **1** indicate the release of loosely

bound water molecules (10% sample weight loss) in the 35−130 °C range, followed by a loss of acid at higher temperatures (the boiling point of CF_3SO_3H is 162 °C). According to the TGA/mass spectroscopy data, water is continuously releasing in the whole temperature range up to 250 °C. The integral water composition of sample **1** corresponds to ca. 18 water molecules per $\{Cr_3O(bdc)_3\}$ unit. Therefore, the resulting formula of **1** could be written as $[Cr_3O(H_2O)_3(bdc)_3]\cdot 6.7TfOH\cdot 15H_2O$.

The chemical composition of the acid in **1** is equal to 4 M TfOH per MIL-101 volume, which is very well consistent with the concentration of the starting aqueous solutions. This implies that the liquid acid solution simply fills the MIL nanopores, without any deviation of the concentrations and notable distortions of the host framework. Such results additionally demonstrate the great stability of the MIL-101 porous framework toward highly acidic media, suggesting potential utilization of similar hybrid compounds in proton-exchange materials and NH_3 capture from industrial exhausts or for acidic heterogeneous catalysis. The ICP-AES spectroscopy analysis of **2** indicates that the S/Cr ratio is 0.37, which could be recalculated to 1.1 TsOH molecule per MIL-101. The TGA data indicate the release of only 2 water molecules per formula unit (ca. 4% weight loss below 130 °C), supporting the formula of **2** as $MIL\text{-}101\cdot 1.1TsOH\cdot 2H_2O$. Surprisingly, low amounts of both TsOH and water guest molecules in **2** could be explained by the low stability of the TsOH@MIL-101 inclusion compound and hampered diffusion. The channels in the MIL-101 structure (11−15 Å) are supposedly plugged by some $TsOH\cdot xH_2O$ aggregates, thus preventing the further inclusion of TsOH or even water molecules in a MIL-101 porous structure. It is to be noted that the TsOH@MIL-101 compound, being exposed to the water vapor for several hours at room temperature, takes up only three additional water molecules, giving rise to $MIL\text{-}101\cdot 1.1TsOH\cdot 5H_2O$ and supporting the idea of poor guest inclusion kinetics due to diffusion difficulties.

The ac impedance measurements of **1** and **2** were carried out by a two-probe method using platinum-pressed electrodes in the temperature range from 25 to 65 °C in air at different humidity conditions: constant 0.6 mol % water (ca. 15% RH at room temperature), constant 3.5 mol % water (100% RH at room temperature), and at constant 50% RH, maintained during the experiments. Typical impedance plots of **2** [see the Supporting Information (SI), Figure S1] feature a part of a semicircle at higher frequencies and a tail at low frequencies at room temperature, which deals with the mobile ions being blocked by the electrode−electrolyte interfaces. The higher-frequency minimum/intercept along the x axis of the impedance plots was used to calculate the bulk resistance of the samples. The temperature dependencies of the proton-conductivity values ($\log \sigma$ vs T^{-1}) for both heating and cooling regimes for **1** and **2** are shown in Figure 2.[37] The shape of the conductivity curve of **1** in the constant molar water atmosphere is almost flat with minor curvature and a maximum near 60 °C. The highest conductivity reaches 0.08 S cm^{-1} at 3.5 mol % water and 0.05 S cm^{-1} at 0.6 mol % water in the atmosphere. The measured proton conductivity of **1** is as high as that of fully hydrated Nafion[4] and, to our best knowledge, exceeds any other solid proton electrolyte at such conditions. There is some discrepancy between the heating and cooling regimes of the measurements, related to the floating water content in the sample during the experiments. The decrease of sample

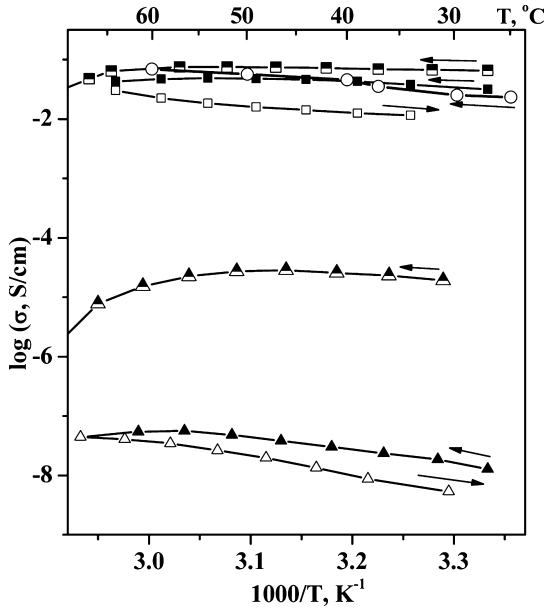

Figure 2. Temperature dependencies of the proton conductivities of **1** (squares) and **2** (triangles). Filled and open symbols indicate heating and cooling measurement regimes, respectively, carried out at 0.6 mol % water vapor. Half-filled symbols mark heating regime data at 3.5 mol % water vapor. Open circles indicate the data for **1** at 50% RH. The lines are drawn to guide the eye.

hydration by heating should affect the proton-conducting network and decrease the proton conductivity. This is apparently negated by an increase of the proton-transfer kinetics at elevated temperatures; therefore, the obtained flat temperature dependencies of the conductivities are reasonable. We should also note here that the temperature- and/or moisture-dependent deviations of the water content of **1** do not change the conductivity values that much because the remaining acid and water guest molecules could maintain a proton-conducting network for the facile proton transfer. The conductivity data measured at constant 50% RH are close to a linear function, increasing with temperature (Figure 2).

The proton conductivity and its moisture-dependent behavior of sample **2** are quite different from those for sample **1**. The measured room temperature conductivity value for **2** at 3.5 mo % water is 1.8×10^{-5}, and it increases up to 3×10^{-5} S cm^{-1} at 50 °C. Further heating leads to a conductivity decrease to 8×10^{-6} S cm^{-1} at 66 °C. Significantly poorer values, compared to **1**, could be explained by the lower acid content, lower pK_a values, and, more importantly, lower water content. Apparently, the limited total guest content in **2** (ca. 12 TsOH and 23 H_2O per MIL-101 nanocage) is not enough to support efficient proton transfer through the extended hydrogen-bonding network. Moreover, the removal of a few more guest water molecules, which takes place at elevated temperature or lower humidity, should break down that network and severely hamper the proton mobility. As a result, the observed curvature of the temperature dependence of the proton conductivity of **2** (Figure 2) is more pronounced, compared to **1**. Also, the measurements at 0.6 mol % water, revealed a dramatic, about 2.5−3 orders of magnitude, decrease of the proton conductivity values below 10^{-7} S cm^{-1} at temperatures over 100 °C. The poor proton conductivity of sample **2** is discouraging; however, materials with such a strong response to the hydration content may find interesting applications, e.g., as a humidity sensor.

dx.doi.org/10.1021/am500438a | ACS Appl. Mater. Interfaces 2014, 6, 5161−5167

The activation energies E_a of proton transport for sample **1** at RH = 50% corresponds to 0.25 eV. Assuming the stable water content of samples **1** and **2** investigated at constant molar humidity, the corresponding activation energies could also be estimated from the Arrhenius equation. The E_a values at low humidity (0.6 mol %) were found to be 0.23 eV for **1** and 0.58 eV for **2** (cooling regime). The first number is very close to 0.25 eV for RH = 50% data and typical for the Grotthuss (relay) mechanism, while the second one could characterize the vehicular mechanism. It is possible, however, that the relay conductivity mechanism dominates in both compounds: the guest-poor **2** requires a significant activation energy for transport through the broken hydrogen-bonding network, contrary to the guest-rich compound **1**. Such convincing discrepancies in the activation energy values and the assumed proton-transfer mechanics justify the relationships between the conducting properties and chemical composition, discussed above. Predictably, the activation energies of the title compound proton transport, calculated for the higher humidity (3.5 mol %) data, are notably lower: $E_a(\mathbf{1}) \approx 0.18$ eV; $E_a(\mathbf{2}) \approx 0.23$ eV. The difference is especially crucial for compound **2**, where the increased sample hydration number in a humid atmosphere seems to "repair" the broken hydrogen-bonding network, making smooth proton transfer between adjacent $H_3O^+\cdots H_2O\cdots TsO^-$ triads through the relay mechanism possible. More importantly, the reduced conductivity values of the compounds heated to 115 °C could be restored to the original values after rehydration in a humid atmosphere (3.5 mol % water) for 6 h at room temperature, ruling out possible acid evaporation. It should be mentioned that no direct evidence of the CF_3SO_3H presence in the gas phase was recorded by mass spectrometry data of **1** at 130 °C (see the SI). Chemical S/Cr analyses also indicate no deviation before and after the conductivity measurements. Therefore, it would be safe to conclude that all changes in the conductivities or possible proton-transfer mechanisms of the samples are related to the variable content of the guest water molecules. In addition to the acid content, the high stability of the MIL-101 crystal structure after multiple proton conductivity measurements of **1** at elevated temperatures (up to 115 °C) was confirmed by PXRD data (see Figure 1 and the SI). The high structural and chemical integrities of the acid-loaded host–guest compounds must impose the stable and reproducible conductivity properties of PEM, based on such hybrid materials, provided that the measurement conditions (temperature and humidity) are maintained on the same level.

Compound **1** with TfOH displays much more attractive proton conductivity properties, so we decided to carry out the in-depth investigation of the proton mobility mechanism by ^{1}H NMR broad-line spectroscopy at lower temperatures between 180 and 290 K. The wide-line NMR spectra of **1**, resulting from magnetic proton–proton and proton–Cr^{3+} interactions, consist of two different lines (Figure 3). The intense narrow symmetric line at the spectrum center belongs to water and acidic protons for which all magnetic interactions are effectively suppressed because of fast (in the NMR time scale) proton migration including guest molecule diffusion and an intermolecular proton exchange. A feeble wide asymmetric line was assigned to immobile proton pairs of terephthalate ions with a H···H distance of ca. 2.5 Å, located between two Cr^{3+} ions with a mean H···Cr^{3+} separation of ca. 4.1 Å (see the SI, Scheme S1). From integral intensities of these lines, the number of mobile protons can be assessed as 48 ± 5 per formula unit, matching

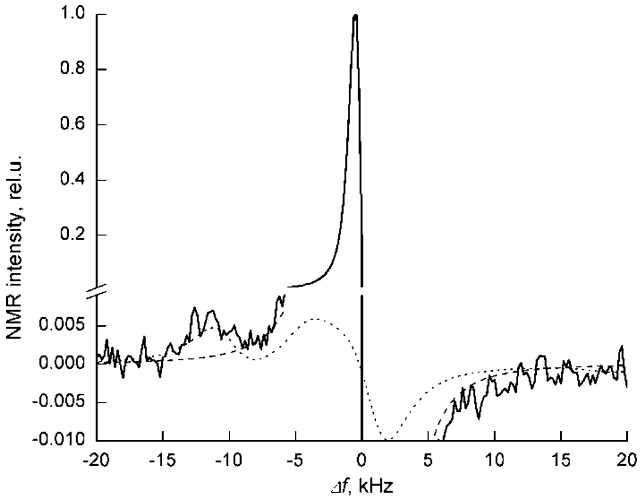

Figure 3. ^{1}H NMR spectrum (the first derivative of the NMR absorption line) for **1** at ambient temperature. The regions of the spectrum, corresponding to $C_8H_4O_4^{2-}$ (bdc), are drawn on an enlarged scale. The NMR trace of water and acidic protons in these regions is shown as a dashed line. The spectrum simulated for the proton pair of bdc, symmetrically located between two Cr^{3+} ions (see the SI), is drawn as a dotted line.

the chemical composition of **1**.[38] The width of the narrow line decreases with the temperature (Figure 4). In the "fast-motion"

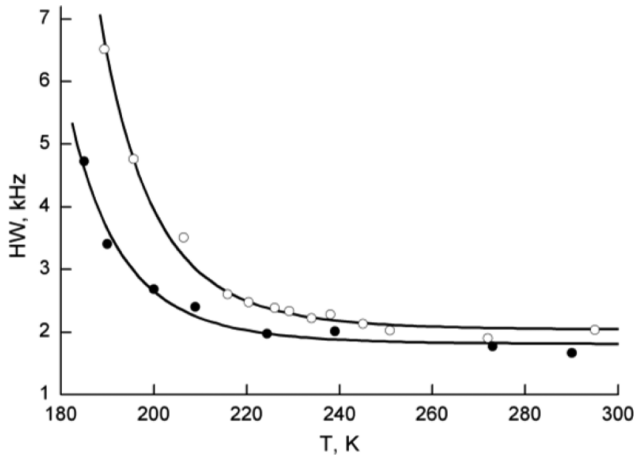

Figure 4. Half-width temperature dependencies of the narrow components of the NMR spectra for **1** (●) and pristine MIL-101 (○). The relevant approximating curves calculated for the activation energies of 0.25 and 0.27 eV are shown as solid lines.

region, the temperature dependence of the NMR line width $\delta\omega$ can be extrapolated by the equation $\delta\omega = \delta\omega_0 + A\exp(E_a/kT)$, where $\delta\omega_0$ is a high-temperature limit of $\delta\omega$ and E_a is the activation energy of the proton mobility.[39] The obtained experimental data correspond to E_a = 0.25 eV and coincide with the values, estimated from the proton-conductivity measurements of **1** at ambient humidity. For reference, similar NMR measurements were conducted for an acid-free MIL-101 compound (Figure 4). The observed $\delta\omega(T)$ dependence is slightly shifted to higher temperatures; however, the calculated activation energy E_a = 0.27 eV is quite comparable. As was mentioned already, such E_a values are close to those of the relay mechanism, which involves proton transfer between adjacent guest species (H_2O, H_3O^+, and TfO^-) and their simultaneous

dx.doi.org/10.1021/am500438a | ACS Appl. Mater. Interfaces 2014, 6, 5161–5167

conformational rotations. On the other hand, the similar dependencies of the NMR line widths upon temperature for both **1** and acid-free MIL-101 imply considerable contribution of water diffusion to the complicated proton-transfer process. On the basis of these observations, the following model of the proton-conducting mechanism inside the MIL-101 nanopores could be proposed that combines both proton-transfer modes. The acid protons are believed to be captured within some spatially isolated water droplets where short-range proton transfer may follow the relay mechanism. Long-range proton migration over all porous structures can become possible if short-range proton exchange is accompanied by a continuous rearrangement of the water droplets in the nanopores due to water molecular diffusion. A similar mechanism was recently considered for proton migration in oxygen-protonated ensembles in the channels of $H[Lu(H_2O)_6\{Re_4Te_4(CN)_{12}\}]\cdot nH_2O$ (E_a = 0.17 eV).[40] We suppose that the proton-migration activation energy for a mechanism of this kind might be basically the activation energy of water self-diffusion rather than the energy barrier for intradroplet Grotthuss-type proton translocation.

A further study of the structure of the proton-conducting network in **1** was carried out by FT-IR measurements in the temperature range of 5−300 K (Figure 5). First, we should mention that the IR peaks of **1** below 2000 cm^{-1}, which mainly correspond to the chromium(III) oxoterephthalate framework, do not show any changes in the whole temperature range. On the contrary, the peaks of O−H stretching vibrations undergo some temperature dependency. A typical room temperature IR spectrum of a water-containing compound, such as **1**, shows broad and featureless peaks in the range 3000−3700 cm^{-1}. The very broad maximum of the IR spectrum of **1** (3310 cm^{-1}) at 300 K is shifted to the lower wavenumber region by ca. 100 cm^{-1}, compared to the liquid water.[41] A similar shift is observed for supercooled water, where it is believed to be attributed to some preordering of the water molecules in a tetrahedral fashion, much like in a crystalline ice.[42−44] This conclusion matches the PXRD data of **1**, viz., a broad background peak (Figure 1), indicating some short-range ordering of the MIL-included species. The temperature decrease below 200 K results in the appearance of a fine structure of distinct water molecules, depending on their local geometry as well as the size, dimension, and chemical environment of the crystalline water clusters. At 5 K, the FT-IR spectra of **1** revealed a complicated peak pattern, centered at ca. 3300 cm^{-1}. The peak structure features a maximum at 3220 cm^{-1} and a number of shoulders, most pronounced at 3070 and 3540 cm^{-1}, and a broad shoulder at ca. 3400 cm^{-1}. Such broadness rules out chainlike crystalline water structures, which could be seen in, e.g., some minerals.[45] The IR spectrum of **1** is also different from the one for bulk crystalline 3D ice, which contains a relatively sharp single peak at 3250 cm^{-1}.[42,44] The shoulder at 3070 cm^{-1}, being absent in normal water or ice, apparently refers to the strong hydrogen-bond interactions involving H_3O^+ cations (e.g., $H_2O{-}H^+\cdots OH_2$ or $H_2O{-}H^+\cdots O_3SCF_3^-$),[46] which must be rather numerous in **1**. Indeed, any hydrogen bonding between a water molecule and some nucleophile (N) HO−H···N weakens and elongates the O−H covalent bond. Stronger hydrogen-bonding interactions exist to an even higher extent, shifting the corresponding IR peak to the lower wavenumber range.

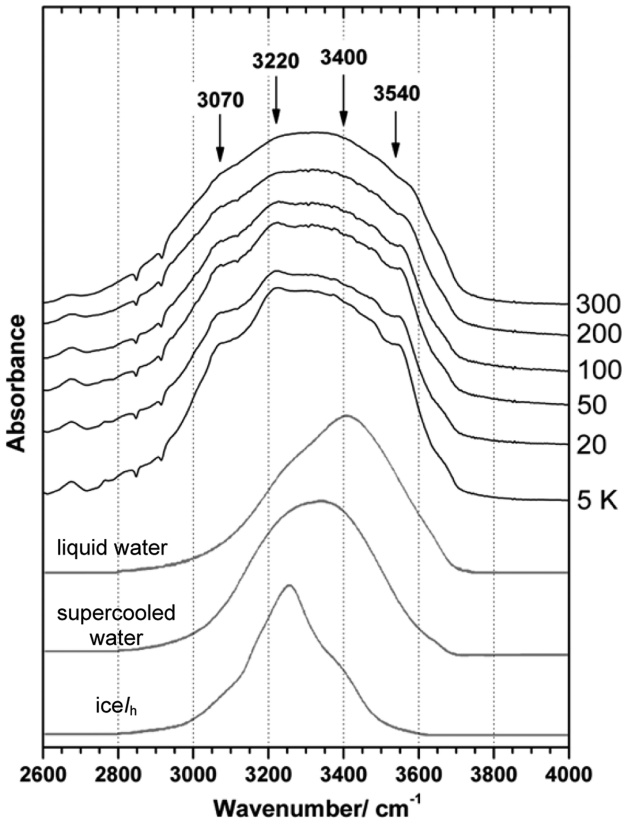

Figure 5. FT-IR spectra of sample **1** recorded at different temperatures (black lines). Arrows indicate selected wavenumbers (cm^{-1}). Gray lines at the bottom refer to the IR spectra of ice, supercooled water, and liquid water.

Compared to the recently studied IR spectra of the various discrete water clusters,[46−49] the spectra of **1** are missing sharp peaks at high wavenumber (ca. 3700 cm^{-1}), which refers to the free O−H stretching. This means that all protons of the aqueous state in **1** participate in hydrogen-bonding interactions between water molecules, $CF_3SO_3^-$ anions, and MIL framework atoms. Three major components of the complex low-temperature IR spectra of **1** (at 3220, 3400, and 3540 cm^{-1}) were previously observed in the large $H^+(H_2O)_n$ ($20 \le n \le 200$) water clusters, featuring similar structures at ca. 3250, 3400, and 3570 cm^{-1}.[49] Most importantly, the size of the water cluster (n) was shown to have a remarkable effect on the relative intensities and the broadness of those components. As much as it could result from the careful spectral comparison, the IR data for **1** at 200 K could be attributed to intermediate size $H^+(H_2O)_n$ water clusters, with n ranging from 40 to 80. This is lower than the average number of 170 water molecules per MIL-101 nanocage, obtained from the chemical composition of **1**, which suggests the coexistence of several water clusters (droplets) in the same nanocage and possible mutual dynamic interplay between them. We must emphasize that the last conclusion strongly supports the hypothesis derived from ^{1}H NMR data analysis. Despite the different time scales of the NMR and FT-IR spectroscopic techniques, both methods engender a quite agreeable model of long-range proton transfer and reveal valuable information about the state of the acidic proton-conducting media inside the MIL-101 pores.

4. CONCLUSIONS

In summary, we demonstrate here that the inclusion of a strong acid, such as TfOH, in the MIL-101 nanopores leads to a solid material with a proton-conductivity value at ambient conditions

of 0.08 S cm^{-1}, similar to that of fully hydrated Nafion. The conducting properties of materials depend on the measurement conditions, such as the temperature and humidity, which actually affects the content of the guest water molecules and the complexity of the hydrogen-bonding network for efficient proton transfer. The materials possess stable crystalline structures that do not deteriorate during the multiple measurements or prolonged heating. According to the spectroscopy data, the MIL-101-encapsulated aqueous solution of TfOH in **1** is composed of large droplets, which have some preorganized structure, facilitated by the regular MIL-101 framework. In the fast snapshot time scale, the droplets are composed of dozens of water molecules with extensive hydrogen-bonding interactions between the guest species and facile relay proton transfer. In the slow time scale, these droplets undergo extensive reorganization, thus assuring the continuous translation diffusion of protons in the materials. Such a dual nature of the conductivity mechanism emphasizes the imminent complexity of long-range proton transfer, which was described for different systems.[50,51]

■ ASSOCIATED CONTENT

Ⓢ Supporting Information

Additional thermogravimetric and thermocalorimetric analyses, mass and FT-IR spectra, and ^{1}H NMR measurements. This material is available free of charge via the Internet at http://pubs.acs.org.

■ AUTHOR INFORMATION

Corresponding Author

*E-mail: cluster@niic.nsc.ru. Tel: +7 (383) 330-94-90. Fax: +7 (383) 330-94-89.

Notes

The authors declare no competing financial interest.

■ ACKNOWLEDGMENTS

This work was partially supported by the Russian Foundation for Basic Research (Grant 12-03-33033) and grants of the RF Government (leading scientist M. Schroder). STA analyses were carried out by K. B. Gerasimov (ISSCM SB RAS). D.N.D. acknowledges the WCU Program through the Korea Science and Engineering Foundation funded by the Ministry of Education, Science and Technology of Korea.

■ REFERENCES

(1) Hickner, M. A.; Ghassemi, H.; Kim, Y. S.; Einsla, B. R.; McGrath, J. E. Alternative Polymer Systems for Proton Exchange Membranes (PEMs). *Chem. Rev.* **2004**, *104*, 4587−4612.

(2) Lee, J. S.; Quan, N. D.; Hwang, J. M.; Lee, S. D.; Kim, H.; Lee, H.; Kim, H. S. Polymer Electrolyte Membranes for Fuel Cells. *J. Ind. Eng. Chem.* **2006**, *12*, 175−183.

(3) Zhang, H.; Shen, P. K. Advances in the High Performance Polymer Electrolyte Membranes for Fuel Cells. *Chem. Soc. Rev.* **2012**, *41*, 2382−2394.

(4) Dupuis, A.-C. Proton Exchange Membranes for Fuel Cells Operated at Medium Temperatures: Materials and Experimental Techniques. *Prog. Mater. Sci.* **2011**, *56*, 289−327.

(5) Barboiu, M.; Cazacu, A.; Michau, M.; Caraballo, R.; Arnal-Herault, C.; Pasc-Banu, A. Functional Organic−Inorganic Hybrid Membranes. *Chem. Eng. Process.* **2008**, *47*, 1044−1052.

(6) Kreuer, K. D.; Schuster, M.; Obliers, B.; Diat, O.; Traub, U.; Fuchs, A.; Klock, U.; Paddison, S. J.; Maier, J. Short-Side-Chain Proton Conducting Perfluorosulfonic Acid Ionomers: Why They Perform Better in PEM Fuel Cells. *J. Power Sources* **2008**, *178*, 499−509.

(7) Kreuer, K. D.; Paddison, S. J.; Spohr, E.; Schuster, M. Transport in Proton Conductors for Fuel-Cell Applications: Simulations, Elementary Reactions, and Phenomenology. *Chem. Rev.* **2004**, *104*, 4637−4678.

(8) Vielstich, Ed. W.; Gasteiger, H. A.; Lamm, A. *Handbook of Fuel Cells—Fundamentals, Technology and Applications*; John Wiley & Sons, Ltd.: London, 2003; Vol. 3, pp 1−3826.

(9) Herring, A. M. Inorganic−Polymer Composite Membranes for Proton Exchange Membrane Fuel Cells. *J. Macromol. Sci., Part C: Polym. Rev.* **2006**, *46*, 245−296.

(10) Kreuer, K. D. On the Development of Proton Conducting Polymer Membranes for Hydrogen and Methanol Fuel Cells. *J. Membr. Sci.* **2001**, *185*, 29−39.

(11) Li, Q.; He, R.; Jensen, J. O.; Bjerrum, N. J. Approaches and Recent Development of Polymer Electrolyte Membranes for Fuel Cells Operating above 100 °C. *Chem. Mater.* **2003**, *15*, 4896−4915.

(12) Alberti, G.; Casciola, M. Solid State Protonic Conductors, Present Main Applications and Future Prospects. *Solid State Ionics* **2001**, *145*, 3−16.

(13) Yuan, J. J.; Pu, H. T.; Yang, Z. L. Studies on Sulfonic Acid Functionalized Hollow Silica Spheres/Nafion® Composite Proton Exchange Membranes. *J. Polym. Sci., Part A: Polym Chem.* **2009**, *47*, 2647−2655.

(14) Li, Q.; Jensen, J. O.; Savinell, R. F.; Bjerrum, N. J. High Temperature Proton Exchange Membranes Based on Polybenzimidazoles for Fuel Cells. *Prog. Polym. Sci.* **2009**, *34*, 449−477.

(15) He, R.; Li, Q.; Xiao, G.; Bjerrum, N. J. Proton Conductivity of Phosphoric Acid Doped Polybenzimidazole and its Composites with Inorganic Proton Conductors. *J. Membr. Sci.* **2003**, *226*, 169−184.

(16) Peighambardoust, S. J.; Rowshanzamir, S.; Amjadi, M. Review of the Proton Exchange Membranes for Fuel Cell Applications. *Int. J. Hydrogen Energy* **2010**, *35*, 9349−9384.

(17) Rikukawa, M.; Sanui, K. Proton-Conducting Polymer Electrolyte Membranes Based on Hydrocarbon Polymers. *Prog. Polym. Sci.* **2000**, *25*, 1463−1502.

(18) Crabtree, G. W.; Dresselhaus, M. S. The Hydrogen Fuel Alternative. *MRS Bull.* **2008**, *33*, 421−428.

(19) Kitagawa, H.; Nagao, Y.; Fujishima, M.; Ikeda, R.; Kanda, S. Highly Proton-Conductive Copper Coordination Polymer, H_2dtoaCu (H_2dtoa = dithiooxamide anion). *Inorg. Chem. Commun.* **2003**, *6*, 346−348.

(20) Yoon, M.; Suh, K.; Natarajan, S.; Kim, K. Proton Conduction in Metal−Organic Frameworks and Related Modularly Built Porous Solids. *Angew. Chem., Int. Ed.* **2013**, *52*, 2688−2700.

(21) Taylor, J. M.; Dawson, K. W.; Shimizu, G. K. H. A Water-Stable Metal−Organic Framework with Highly Acidic Pores for Proton-Conducting Applications. *J. Am. Chem. Soc.* **2013**, *135*, 1193−1196.

(22) Goesten, M. G.; Juan-Alcañiz, J.; Ramos-Fernandez, E. V.; SaiSankar Gupta, K. B.; Stavitski, E.; Van Bekkum, H.; Kapteijn, F. Sulfation of Metal−Organic Frameworks: Opportunities for Acid Catalysis and Proton Conductivity. *J. Catal.* **2011**, *281*, 177−187.

(23) Shigematsu, A.; Yamada, T.; Kitagawa, H. Wide Control of Proton Conductivity in Porous Coordination Polymers. *J. Am. Chem. Soc.* **2011**, *133*, 2034−2036.

(24) Jeong, N. C.; Samanta, B.; Lee, C. Y.; Farha, O. K.; Hupp, J. T. Coordination-Chemistry Control of Proton Conductivity in the Iconic Metal−Organic Framework Material HKUST-1. *J. Am. Chem. Soc.* **2012**, *134*, 51−54.

(25) Kim, S.; Dawson, K. W.; Gelfand, B. S.; Taylor, J. M.; Shimizu, G. K. H. Enhancing Proton Conduction in a Metal−Organic Framework by Isomorphous Ligand Replacement. *J. Am. Chem. Soc.* **2013**, *135*, 963−966.

(26) Colodrero, R. M. P.; Olivera-Pastor, P.; Losilla, E. R.; Hernández-Alonso, D.; Aranda, M. A. G.; Leon-Reina, L.; Rius, J.; Demadis, K. D.; Moreau, B.; Villemin, D.; Palomino, M.; Rey, F.; Cabeza, A. High Proton Conductivity in a Flexible, Cross-Linked, Ultramicroporous Magnesium Tetraphosphonate Hybrid Framework. *Inorg. Chem.* **2012**, *51*, 7689−7698.

(27) Costantino, F.; Donnadio, A.; Casciola, M. Survey on the Phase Transitions and Their Effect on the Ion-Exchange and on the Proton-Conduction Properties of a Flexible and Robust Zr Phosphonate Coordination Polymer. *Inorg. Chem.* **2012**, *51*, 6992−7000.
(28) Hurd, J. A.; Vaidhyanathan, R.; Thangadurai, V.; Ratcliffe, C. I.; Moudrakovski, I. L.; Shimizu, G. K. H. Anhydrous proton conduction at 150 °C in a crystalline metal−organic framework. *Nat. Chem.* **2009**, *1*, 705−710.
(29) Umeyama, D.; Horike, S.; Inukai, M.; Hijikata, Y.; Kitagawa, S. Confinement of Mobile Histamine in Coordination Nanochannels for Fast Proton Transfer. *Angew. Chem., Int. Ed.* **2011**, *50*, 11706−11709.
(30) Bureekaew, S.; Horike, S.; Higuchi, M.; Mizuno, M.; Kawamura, T.; Tanaka, D.; Yanai, N.; Kitagawa, S. One-Dimensional Imidazole Aggregate in Aluminium Porous Coordination Polymers with High Proton Conductivity. *Nat. Mater.* **2009**, *8*, 831−836.
(31) Ōkawa, H.; Sadakiyo, M.; Yamada, T.; Maesato, M.; Ohba, M.; Kitagawa, H. Proton-Conductive Magnetic Metal−Organic Frameworks, $\{NR_3(CH_2COOH)\}[M_a^{II}M_b^{III}(ox)_3]$: Effect of Carboxyl Residue upon Proton Conduction. *J. Am. Chem. Soc.* **2013**, *135*, 2256−2262.
(32) Horike, S.; Kamitsubo, Y.; Inukai, M.; Fukushima, T.; Umeyama, D.; Itakura, T.; Kitagawa, S. Postsynthesis Modification of a Porous Coordination Polymer by LiCl To Enhance H^+ Transport. *J. Am. Chem. Soc.* **2013**, *135*, 4612−4615.
(33) Ponomareva, V. G.; Kovalenko, K. A.; Chupakhin, A. P.; Dybtsev, D. N.; Shutova, E. S.; Fedin, V. P. Imparting High Proton Conductivity to a Metal−Organic Framework Material by Controlled Acid Impregnation. *J. Am. Chem. Soc.* **2012**, *134*, 15640−15643.
(34) Férey, G.; Mellot-Draznieks, C.; Serre, C.; Millange, F.; Dutour, J.; Surblé, S.; Margiolaki, I. A Chromium Terephthalate-Based Solid with Unusually Large Pore Volumes and Surface Area. *Science* **2005**, *309*, 2040−2042.
(35) Kreuer, K.-D.; Wohlfarth, A. Limits of Proton Conductivity. *Angew. Chem., Int. Ed.* **2012**, *51*, 10454−10456.
(36) Aihara, Y.; Sonai, A.; Hattori, M.; Hayamizu, K. Ion Conduction Mechanisms and Thermal Properties of Hydrated and Anhydrous Phosphoric Acids Studied with ^1H, ^2H, and ^{31}P NMR. *J. Phys. Chem. B* **2006**, *110*, 24999−25006.
(37) Because of the liquid nature of the acidic solutions, some contribution of the acid solution between MIL-101 crystallites to the total sample conductivity is inevitable. This contribution, however, could be estimated as the ratio between the "inner" and "outer" surfaces of the MIL-101 octahedral crystallites. Given the average crystallite size (ca. 250 nm) and the crystallographic density of MIL-101 (0.514 g cm^{-3}), the external surface area equals ca. 60 $m^2\ g^{-1}$, which is less than 2% of the total MIL-101 surface area (3200 $m^2\ g^{-1}$).
(38) On the basis of the formula unit composition of **1**, which is $[Cr_3O(H_2O)_3(bdc)_3]\cdot 6.7CF_3SO_3H\cdot 15H_2O$, the amount of mobile protons could be calculated as $3 \times 2 + 6.7 + 15 \times 2 \approx 43$.
(39) Abragam, A. *The Principles of Nuclear Magnetism*; Clarendon Press: Oxford, U.K., 1961; pp 1−599.
(40) Efremova, O. A.; Golenkov, E. O.; Mironov, Y. V.; Moroz, N. K.; Wang, C.; Fedorov, V. E. Proton Transfer in a New Chain-Like Cluster Compound $H[Lu(H_2O)_6\{Re_4Te_4(CN)_{12}\}]\cdot 6H_2O$. *J. Phys. Chem. C* **2007**, *111*, 11008−11011.
(41) Bertie, J. E.; Lan, Z. Infrared Intensities of Liquids XX: The Intensity of the OH Stretching Band of Liquid Water Revisited, and the Best Current Values of the Optical Constants of H_2O(l) at 25 °C. *Appl. Spectrosc.* **1996**, *50*, 1047−1057.
(42) Delvin, J. P. Polarized Raman Spectra for the Full Range of Isotopic Dilution for Ice and Amorphous Ice: Mixtures of Intact H_2O and D_2O. *J. Chem. Phys.* **1989**, *90*, 1322−1329.
(43) Sivakumar, T. C.; Rice, S. A.; Sceats, M. G. Raman Spectroscopic Studies of the OH Stretching Region of Low Density Amorphous Solid Water and of Polycrystalline Ice Ih. *J. Chem. Phys.* **1978**, *69*, 3468−3476.
(44) Zasetsky, A. Y.; Khalizov, A. F.; Earle, M. E.; Sloan, J. J. Frequency Dependent Complex Refractive Indices of Supercooled Liquid Water and Ice Determined from Aerosol Extinction Spectra. *J. Phys. Chem. A* **2005**, *109*, 2760−2764.
(45) Kolesov, B. A.; Geiger, C. A. Raman Spectroscopic Study of H_2O in Bikitaite: "One-Dimensional Ice". *Am. Mineral.* **2002**, *87*, 1426−1431.
(46) 2655 cm^{-1} for $H^+\cdot(H_2O)_4$, 2860 cm^{-1} for $H^+\cdot(H_2O)_5$, 3160 cm^{-1} for $H^+\cdot(H_2O)_6$ in: Headrick, J. M.; Diken, E. G.; Walters, R. S.; Hammer, N. I.; Christie, R. A.; Cui, J.; Myshakin, E. M.; Duncan, M. A.; Johnson, M. A.; Jordan, K. D. Spectral Signatures of Hydrated Proton Vibrations in Water Clusters. *Science* **2005**, *308*, 1765−1769.
(47) Miyazaki, M.; Fujii, A.; Ebata, T.; Mikami, N. Infrared Spectroscopic Evidence for Protonated Water Clusters Forming Nanoscale Cages. *Science* **2004**, *304*, 1134−1137.
(48) Shin, J.-W.; Hammer, N. I.; Diken, E. G.; Johnson, M. A.; Walters, R. S.; Jaeger, T. D.; Duncan, M. A.; Christie, R. A.; Jordan, K. D. Infrared Signature of Structures Associated with the $H^+(H_2O)_n$ (n = 6 to 27) Clusters. *Science* **2004**, *304*, 1137−1140.
(49) Mizuse, K.; Mikami, N.; Fujii, A. Infrared Spectra and Hydrogen-Bonded Network Structures of Large Protonated Water Clusters $H^+(H_2O)_n$ (n = 20−200). *Angew. Chem., Int. Ed.* **2010**, *49*, 10119−10122.
(50) Kreuer, K. D. On the Complexity of Proton Conduction Phenomena. *Solid State Ionics* **2000**, *136−137*, 149−160.
(51) Paddison, S. J. Proton Conduction Mechanisms at Low Degrees of Hydration in Sulfonic Acid-Based Polymer Electrolyte Membranes. *Annu. Rev. Mater. Res.* **2003**, *33*, 289−319.